ACS APPLIED MATERIALS & INTERFACES

Research Article

www.acsami.org

Sodium Hexadecyl Sulfate as an Interfacial Substance Adjusting the Adsorption of a Protein on Carbon Nanotubes

Jian Sun,[†,§] Kun Du,[†,§] Li Fu,[‡] Jiang Gao,[‡] Haiyang Zhang,[†] Wei Feng,*[,†] and Peijun Ji*[,‡]

[†]Beijing Key Lab of Bioprocess, Department of Biochemical Engineering and [‡]Department of Chemical Engineering, Beijing University of Chemical Technology, Beijing, 100029, China

Supporting Information

ABSTRACT: Carbon nanotubes (CNTs) were functionalized with sodium hexadecyl sulfate (SHS). The lysozyme adsorbed on the SHS-CNTs exhibited a higher activity than that immobilized on the nonfunctionalized CNTs. To explain the experimental results and explore the mechanism of lysozyme adsorption, large-scale molecular dynamics simulations have been performed for a four-component system, including lysozyme, SHS, CNTs in explicit water. It has been found that the assembled SHS molecules form a soft layer on the surface of CNTs. The interactions between lysozyme and SHS induce the rearrangement of SHS molecules, forming a saddle-like structure on the CNT surface. The saddle-like structure fits the shape of the lysozyme, and the active-site cleft of the lysozyme is exposed to the water phase. Whereas, for the lysozyme adsorbed on the nonfunctionalized CNT, due to the hydrophobic interactions, the active-site cleft of the enzyme tends to face the wall of the CNT. The results of this work demonstrate that the SHS molecules as the interfacial substance have a function of adjusting the lysozyme with an appropriate orientation, which is favorable for the lysozyme having a higher activity.

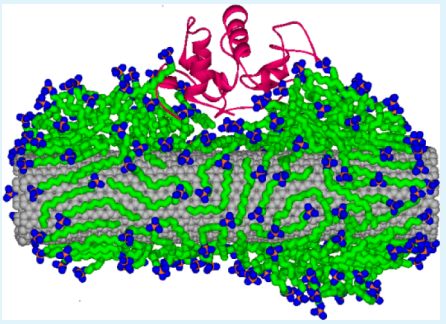

KEYWORDS: *sodium hexadecyl sulfate, lysozyme, carbon nanotubes, molecular dynamics simulation*

1. INTRODUCTION

Nanomaterials have been extensively investigated as supporting materials for the adsorption of proteins, because nanoscale materials can provide high surface area for effective loading and reduced diffusion limitations.[1,2] Carbon nanotubes (CNTs) exhibit distinct properties, including extraordinary mechanical, electrical, and thermal properties, as well as biocompatible properties.[3] CNTs have been extensively investigated for enzyme immobilization.[4,5] Enzyme immobilization is a promising biotechnological application of CNTs.[6]

van der Waals interactions between the sidewalls of individual pristine CNTs lead to the formation of bundles.[7] Functionalized CNTs can be well-dispersed in biocompatible media, facilitating their biological applications.[2,3] Surfactants have been utilized to disperse CNTs in aqueous solutions.[8−10] Surfactants are self-assembled around the CNTs, and the CNT/surfactant complex is highly hydrophilic.[11] Streptavidin was specifically bound to the Triton X-100 functionalized CNTs.[12] Enzymes and surfactants together have been adsorbed onto CNTs,[13] and enhanced faradic responses were achieved. For selective immobilization of enzymes, two surfactants have been adsorbed onto CNTs.[14] The solution of sodium cholate was used to disperse CNTs,[15] and [FeFe] hydrogenase was bound to the CNTs by displacing the sodium cholate.

As a model protein, lysozyme has been extensively investigated for the interaction with carbon nanoparticles.[16] Adsorption of the lysozyme on CNTs makes the CNTs water-soluble, the conjugate of lysozyme and CNTs can be well-dispersed in aqueous solutions.[17−21] The secondary structure of the lysozyme adsorbed on CNTs has been preserved well.[17,22] Lysozyme-functionalized CNTs can spun into fibers in the presence of cationic surfactants,[23] exhibiting antibacterial and mechanical properties. Interactions between carbon nanotubes and lysozyme has been studied experimentally.[19] Molecular dynamics (MD) simulation has been proved to be a powerful tool to gain insight into the interactions between proteins and CNTs.[16,24−28] The favorite adsorption site of the lysozyme on the CNT and the protein−tube interaction region has been indicated.[24] The simulations for the lysozyme adsorption on a hydrophobic flat graphite surface[27] and on the CNTs[28] indicated that the lysozyme adsorption strength is dependent on the surface topography.

In this work, CNTs were functionalized with an ionic surfactant (sodium hexadecyl sulfate, SHS) and the functionalized CNTs were utilized to adsorb lysozyme. Parallel work has been carried out for the adsorption of lysozyme on the nonfunctionalized CNTs. It has been found that the enzymatic activity of the lysozyme-SHS-CNTs is much higher than the lysozyme-CNTs. MD simulations have been performed to interpret the experimental results and to investigate the mechanism of lysozyme adsorption. MD simulations will reveal that the SHS molecules rearrange themselves to fit the shape of

Received: May 26, 2014
Accepted: August 15, 2014
Published: August 15, 2014

the lysozyme, leading to the adsorbed lysozyme with an appropriate position that is favorable for the enzymatic catalysis.

2. MATERIALS AND METHODS

2.1. Materials. Multiwalled carbon nanotubes (MWNTs) were purchased from Nanotech Port Co., Ltd. (Shenzhen, China), with a purity of >95%. Sodium hexadecyl sulfate (SHS), lysozyme, *Micrococcus lysodeikticus* cells, and sucrose were purchased from Sigma–Aldrich Chemical Co., China. Sulfuric acid, nitric acid, ferric nitrate, and 2-propanol were purchased from Sinopharm Chemical Reagent Co. All chemicals are analytical grade or higher, and they were used as-received without any further purification. Deionized double-distilled water was used in the preparation of the solutions.

2.2. Experimental Measurements. *Preparation of Magnetic MWNTs.* MWNTs were purified and oxidized as reported elsewhere.[29] By refluxing in a nitric acid solution (2.6 M), the purification of MWNTs was carried out at 70 °C for 45 h. By filtering through a polycarbonate membrane (0.8 μm), the suspensions of MWNTs were washed with double-distilled water. Oxidation of the purified MWNTs was carried out in a H_2SO_4/HNO_3 mixture (3:1) for 3 h. The polycarbonate membrane (0.45 μm) was utilized to filter the oxidized MWNTs, rinsing with double-distilled water. The final samples were obtained through vacuum drying at 80 °C.

Methods described in the literature[30] were used to prepare magnetic MWNTs (M-MWNTs). The solution, consisting of 1.0 g of H_2O, 0.1 g of H_2SO_4 (98%), 0.23 g of sucrose, and 1.5 g of $Fe(NO_3)_3{\cdot}9H_2O$, was prepared. The oxidized MWNTs were impregnated through dropwise addition of this solution. The impregnated samples were dried at 120 °C. They were further treated under nitrogen at 450 °C for 2 h.

Determination of the Amount of SHS Adsorbed. Malachite green (MG) can form a complex with SHS, as shown in Scheme S1 in the Supporting Information; within the pH range of 4.00–6.50, the complex is quite stable. The SHS solutions were prepared with various concentrations, including 0.4. 0.8. 1.2. 1.6. 2.0. 2.4 mg/mL. In preparing the samples, 3 mL of the SHS solution was used and the amount of MG was calculated according to a 1:1 molar ratio. The pH of the mixture was adjusted to be 5.0 by adding acetic acid. Ten milliliters (10 mL) of chloroform was added to the mixture and stirred under shaking for 10 min. Then, another 10 mL of chloroform was added and the mixture was equilibrated for 20 min. The absorbance of the chloroform phase, in which the MG/SHS complex was extracted, was measured at 616 nm. The obtained calibration curve is shown in Figure S1 in the Supporting Information.

Adsorption of the Surfactant SHS on M-MWNTs. Sixty milligrams (60 mg) of surfactant SHS was added to the 2-propanol/water solution (40 mL volume, concentration = 15%). The mixture was sonicated for 20 min, and then 20 mg of M-MWNTs was added. Further sonication was carried out for 1 h. The SHS-functionalized M-MWNTs were separated from the mixture by centrifugation at 12 000 rpm for 30 min.

Saturation Adsorption of the Lysozyme onto the SHS-Functionalized M-MWNTs. The concentrations of the lysozyme solutions ranged from 0.02 mg/mL to 0.15 mg/mL. The solution of SHS-functionalized M-MWNTs was prepared with a concentration of 0.075 mg/mL. The lysozyme solutions were added to the CNTs solution, and then the mixtures were shaken at 4 °C in an incubator shaker at 150 rpm for 4 h. The concentrations of lysozyme in the solutions were determined using the micro bicinchoninic acid assay.[30] The solutions with a concentration range from 0.0 to 0.80 mg/mL were prepared for measurement of the standard curve. Twenty microliters (20 μL) of each protein standard solution and each unknown sample were pipetted into a 96-well micro plate. Two hundred microliters (200 μL) of the BCA working reagent was added to each well, and the plate was mixed thoroughly on a plate shaker for 30 min. The plate was incubated at 37 °C for 30 min. Using an automated microplate reader, the absorbance at 562 nm was recorded for the plates. For each unknown sample, the concentration was determined using the protein standard curve. By detecting the protein remaining in the supernatant, the amount of lysozyme adsorbed onto the SHS-functionalized M-MWNTs was determined. Average values were obtained from triplicate measurements of three adsorption operations. Similar procedures were used to measure the adsorption of lysozyme on the nonfunctionalized M-MWNTs. The contents of lysozyme adsorbed are 0.48 mg/mg CNTs and 0.32 mg/mg CNTs for SHS-M-MWNTs and for M-MWNTs, respectively. The relative changes in adsorption capacities are below 2.15%.

Optical Spectroscopy. Ultraviolet–visible (UV-vis) spectra were measured in a Shimadzu Model UV2550-PC spectrophotometer, using 1-cm-path-length quartz cuvettes. Spectra were collected within a range of 190–800 nm.

For measuring infrared spectra, a Fourier transform infrared (FTIR) spectrometer (Bruker TENSOR 27) was used, which was equipped with a horizontal, temperature-controlled attenuated total reflectance (ATR) device with a ZnSe crystal (Pike Technology). Mercury–cadmium–telluride detector was used. Each spectrum was collected at a resolution of 2 cm^{-1} with 128 scans. Corrected FTIR spectra were obtained by subtracting the background of the ATR element spectrum. Ultrapure nitrogen gas was introduced to purge water vapor.

By measuring circular dichroism (CD) spectra, the secondary structures of the free lysozyme and lysozyme/SHS-CNTs were monitored. CD data were collected with a JASCO instrument (Model J-810). The CD data were measured at a scan speed of 50 nm/min. The cell length was 10 mm. The lysozyme concentration was kept at 50 μg/mL, and CD measurements were carried out at 25 °C.

Lytic Activity of Lysozyme. The rate of lysis of *Micrococcus lysodeikticus* by the lysozyme was measured as reported.[31] The activity of the lysozyme was measured using spectrophotometric turbidity assay. The lysozyme was added into the potassium phosphate buffer (66 mM, pH 6.2) in vials, and the mixture was shaken for 2 h at 4 °C. The lysozyme concentration was 50 μg/mL. The *Micrococcus lysodeikticus* solution was prepared in the potassium phosphate buffer (66 mM), and the concentration was 0.3 mg/mL. In the cuvette, 0.2 mL of the lysozyme solution was mixed with 4.0 mL of the *Micrococcus lysodeikticus* solution. The absorbance at 450 nm was recorded on a Shimadzu Model UV-vis 2500 spectrophotometer at 30 °C, and the data were used to calculate the extent of the hydrolysis of the cell wall substrate. Triplicate measurements were carried out to obtain the average values.

The conjugate SHS-M-MWNTs immobilized more lysozyme than the nonfunctionalized M-MWNTs. In order to compare the enzyme activity on the same basis, the relative activity of the immobilized lysozyme was used. The relative activity is defined as the ratio of the activity of immobilized lysozyme to the activity of free lysozyme. Through the BCA method, the amount of lysozyme immobilized was determined. Both the activity of free lysozyme and that of immobilized lysozyme were measured. To measure the activity of free lysozyme, the amount of free enzyme used is equivalent to the amount of lysozyme immobilized. The relative activity is the retained activity by the immobilized lysozyme.

2.3. Molecular Dynamics Simulation. The crystal structure (7LYZ) was used as the initial structure of the lysozyme, which was taken from the Protein Data Bank. It is composed of a peptide chain containing 129 amino acid residues that form four α-helical segments: one 3_{10} helix and one three-stranded antiparallel β-sheet with four disulfide bridges. The optimal pH for lysozyme is pH ~6.2; under this pH condition, the lysozyme exhibits maximal enzymatic activity.[32] The H++ program[33] was applied to calculate protonation states of titratable groups at pH 6.2.

The VMD software was used to generate a coordinate of carbon nanotube with a chiral index (15,15). For the lysozyme–SHS–CNT system, the carbon nanotube is 10.0 nm long with a diameter of 2.03 nm. For the system lysozyme–CNT, the CNT is 10.0 nm long with a diameter of 4.0 nm. The parameters for the CNT are the same as that in our previous work.[26] The geometric parameters and potential parameters for SHS were obtained from the Dundee PRODRG server,[34] and the charge parameters were derived from Schweighofer.[35]

The partial charges for isopropanol were download from ATB (http://compbio.chemistry.uq.edu.au/atb/index.py).

The GROMACS software package (version 4.5.4)[36] was applied to carry out molecular dynamics (MD) simulations. The Gromos96 45a3 force field was adopted.[37] For the systems of free lysozyme and CNT−lysozyme, the explicit SPCE water was used,[26,38] and eight Cl^- ions were added to neutralize the system charge. Sufficient water molecules were included in the simulations, ensuring the presence of a water bulk phase around the SHS−CNT or SHS−CNT−lysozyme. Steepest descent energy minimization were carried out for the systems. For the MD simulations, a time step was 2 fs, and coordinates of lysozyme were saved every 0.5 ps for later analysis. A Berendsen-type algorithm[39] was used to control temperature and pressure, and the coupling constants were 0.1 and 0.5 ps, respectively. The particle-mesh-Ewald algorithm[40] was used to calculate the electrostatic interactions. The interpolation order was 6, and the grid spacing was 1.2 Å. The cutoff for van der Waals interactions was 14 Å. During the MD simulations, the CNT coordinates were fixed, while those of the lysozyme, SHS, water, and ions were allowed to move. MD simulations were carried out at 1 bar and 323 K. The temperature and pressure conditions correspond to the experimental conditions. MD simulations for the self-assembly of SHS on the CNT were performed for 100 ns in the solution of water and isopropanol (85:15 (vol %)). The trajectories from the 100th nanosecond simulation were used as the starting structure for another 100 nanosecond simulations for the adsorption of lysozyme on the CNT in water.

Potential of mean force (PMF) calculation was carried out according to the literature.[41] For the process of lysozyme adsorption, the free energy, enthalpy, and entropy were extracted from the PMF profile. The umbrella sampling method[42] was used to calculate the PMFs. A harmonic potential was applied through the center of mass of lysozyme at the ith window with a size of 0.1 nm along the x-coordinate, and a set of separate umbrella simulations were performed. The harmonic potentials were expressed by

$$w_i(x_i) = \frac{1}{2}k(x - x_i)$$

where k is the force constant, x the coordinate of the lysozyme, and x_i the center position of the ith window. The initial position of the center of lysozyme is located 3.1 nm from the center of CNT, and the last position is located 6.4 nm from the center of CNT. To cover this distance, 34 independent configurations for 34 windows were generated. For each window, an equilibrium run was performed for 10 ns, and then an additional 10 ns production run was carried out. Analysis of results was performed with the weighted histogram analysis method.[43]

3. RESULTS AND DISCUSSION

3.1. Adsorption of SHS on Carbon Nanotubes. *Experimental Results.* The carbon nanotubes (CNTs) were oxidized by sulfuric and nitric acids, and negative charges (carboxylate groups) on their surface were introduced. The negative charges interact with Fe(III) ions in the solution through electrostatic interactions,[44,45] and nucleation sites for the iron oxide were generated. As can be seen in Figure S2 in the Supporting Information, magnetic nanoparticles are attached on the CNT, but most of the area of the CNT surface was uncovered, which exhibits hydrophobic properties. The adsorption of SHS molecules on the magnetic CNTs confirms that the hydrophobic interactions happened between the tails of SHS and the surface of the CNTs. From this point, it can be concluded that the effect of decorated magnetic nanoparticles on the adsorption of SHS surfactant is limited.

Compared to the transmission electron microscopy (TEM) image of purified CNTs (see Figure S2a in the Supporting Information), in the TEM image of SHS-functionalized CNTs (Figure S2b in the Supporting Information), a thin layer is clearly observed, which is due to the adsorption of SHS molecules. The functionalization of M-MWNTs was also confirmed by the FTIR spectra illustrated in Figure S3 in the Supporting Information. The two intense bands at ∼2917 and 2850 cm^{-1} were assigned to asymmetric and symmetric stretching vibration of $C-CH_2$ from the methylene chain, respectively. The band at 1176 cm^{-1} is due to S═O of SHS. The conjugate of M-MWNTs with the surfactant can be easily separated from the solution by utilizing a magnet (see Figure S4 in the Supporting Information). Alcohol solutions have been found to promote the assembly of a sugar-based surfactant on CNTs.[46] Alcohols are co-solvents for surfactants.[47] For ionic surfactants, alcohols can destabilize micelles by displacing water from the surface, therefore decreasing its effective dielectric constant, increasing headgroup repulsions, and disrupting surfactant packing.[48] When redispersing in water, the dispersibility of the functionalized M-MWNTs was evaluated by measuring the UV-vis spectra. A higher UV-vis absorbance means a larger aqueous dispersibility of the functionalized M-MWNTs. It was found that the M-MWNTs functionalized in the 2-propanol solution with a concentration of 15% (v:v) had the largest dispersibility in water (see Figure S5 in the Supporting Information). The good water dispersibility facilitates the adsorption of proteins on the functionalized M-MWNTs.

Simulation Results. Figure 1 shows the side view and front view of the representative equilibrium snapshots for the SHS

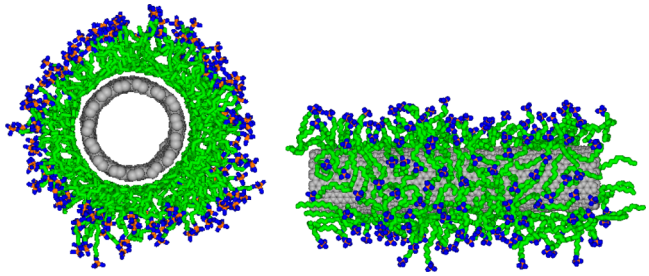

Figure 1. Representative simulation snapshots of equilibrated SHS−CNT aggregate (CH_n− groups in surfactant tails are shown as green lines, sulfur atoms in surfactant heads appear as orange spheres, and oxygen atoms in surfactant heads are shown as blue spheres). CNT is shown in gray. Water molecules have been removed for clarity.

adsorption configuration on the CNT surface with a packing density of SHS of 2.90 SHS molecules/nm^2, corresponding to the experimental concentration ratio of SHS to CNTs. The hydrophobic interactions between the hydrophobic chains and the wall of CNT are the driving force for the adsorption of SHS, and the tail groups of SHS are close to the nanotube surface. The assembly of SHS molecules on the CNT was driven by chain−chain interactions, and most of the head groups are nearly vertically oriented against the surface and extend to the outer aqueous phase. The simulated morphology SHS is similar to that for sodium dodecyl sulfate (SDS).[11]

3.2. Lysozyme Adsorption on SHS-Functionalized CNTs. *Experimental Results.* The method for the adsorption of lysozyme onto the functionalized M-MWNTs has been described in detail in the Supporting Information. The TEM image (Figure S2c in the Supporting Information) shows the conjugate of SHS-M-MWNT with lysozyme, which can be easily separated from the solution by utilizing a magnet (Figure S4 in the Supporting Information). The separation was carried

out without causing any loss of the protein remaining in the solution, exhibiting advantages over the methods such as filtration through membranes and precipitation by centrifugation. Thus, the amount of lysozyme remaining in the solution was determined through the BCA method[49] with a high precision. To measure the amount of lysozyme adsorbed on the CNTs, average values were taken from triplicate measurements of three adsorption operations, and the relative changes in lysozyme adsorption capacities are less than 2.2% ± 0.4%.

Circular dichroism (CD) spectroscopy is extensively applied to monitor the secondary structure and conformation of proteins in solutions.[50] CD spectra can be used to estimate the fraction of the residues in the protein structure that are involved in α-helix and β-sheet. In order to understand the conformational changes of lysozyme induced by the adsorption, we studied the CD spectra of the lysozyme after adsorption. Figure S6 in the Supporting Information represents the CD spectra of free and adsorbed lysozyme. The CD spectrum of free lysozyme shows a minima at 208, indicating the existence of α-helix present in the protein. The line (red) for the lysozyme adsorbed has kept the shape of the line (black) for the free lysozyme, the two lines are close to each other. It is indicative of that the secondary structure of the lysozyme has been preserved well during adsorption.

Simulation Results. There are 6 Lys and 11 Arg residues presented on the surface of the enzyme. At pH 6.2, the Arg and Lys residues of the lysozyme are at protonation states. The head groups of SHS adsorbed on CNT are negatively charged. For selecting initial orientations of the lysozyme, the distribution of Arg and Lys residues on the surface of the protein and the steric hindrance for the adsorption were taken into account. Finally, seven initial orientations toward the functionalized CNT were selected, as illustrated in Figure S7 in the Supporting Information. Compared to other orientations, orientation 6 had the largest interaction energy between the lysozyme and SHS (Figure S8a in the Supporting Information). Orientation 6 was finally selected for the analysis of molecular dynamics simulations.

Potential of Mean Force (PMF) Analysis. PMF calculations were used to examine the changes of system energy as a function of the distance between the center of mass of the CNT and that of the lysozyme. The profile of the PMF versus distance (d) is shown in Figure 2, starting from d = 3.1 nm to d = 6.4 nm. The distance d is specified as the inset in Figure 2. As d > 6.0, the PMF value is almost zero, indicating that the interactions between the SHS-CNT and lysozyme have been significantly reduced. The values of PMF increase with the distance d when d < 6.0 nm, indicating a spontaneous process for the lysozyme adsorption

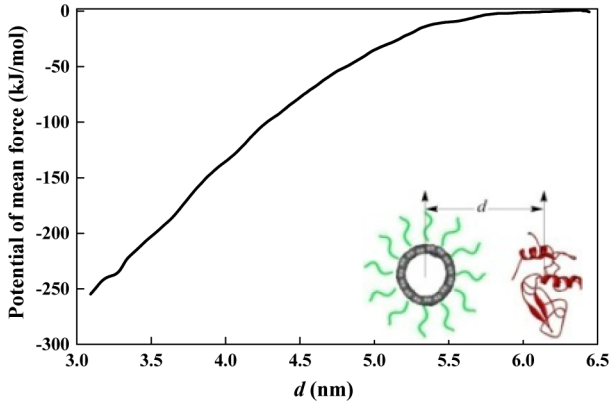

Figure 2. PMF profile versus distance d is the distance between the mass center of CNT and that of lysozyme.

Free-Energy Components. The free energy (ΔG) is given as

$$\Delta G = \Delta H - T\Delta S = \Delta E + P\Delta V - T\Delta S$$

where ΔH, ΔE, ΔS, and ΔV are the changes in enthalpy, internal energy, entropy, and volume of the system, respectively.

For the systems investigated, ΔV is negligible, compared with ΔE (see Figure S9a in the Supporting Information). The internal energy consists of the potential energy E_p and the kinetic energy E_k. There is a little change in the kinetic energy E_k for each umbrella sampling window (see Figure S9b in the Supporting Information), and ΔE_p can be approximated to be ΔH. The potential energy variation, with respect to the distance d, is presented in Figure S10a in the Supporting Information; it shows that the variation trend of the potential energy curve is in accordance with the free-energy profile, implying that the lysozyme adsorption is dominated by enthalpy. Bonded and nonbonded interactions contribute to the potential energy E_p of the system. The change in the bonded interaction energy (Figure S10a in the Supporting Information) is rather small, while there is a significant variation of the magnitude in the nonbonded interactions (Figure S10b in the Supporting Information).

With the lysozyme approaching to the CNT (d decreasing), the total entropy is decreased (Figure 3). The components of lysozyme, SHS and water have different contributions to the entropy change. The entropy of water is increased. At initial states, water molecules were solvated around the SHS molecules and the lysozyme in an ordered structure. During the lysozyme approaching to the CNT, the interactions of SHS with water have to be destroyed due to the stronger interactions of lysozyme with SHS. As a result, the water molecules move out of the interval region and finally water molecules are found at the interval region shorter than 1.6 nm, as illustrated in Figure 4. This results in an increased entropy of water molecules, which is favorable for the lysozyme adsorption. The interaction between lysozyme and SHS provides less freedom for lysozyme and SHS. This leads to that the entropy of lysozyme and SHS are decreased with d decreasing. The PMF profile (Figure 2) indicates that the

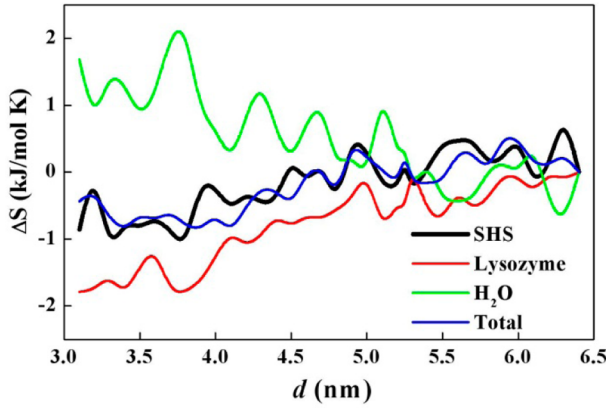

Figure 3. Changes in the entropy of every components of the system over the lysozyme position.

dx.doi.org/10.1021/am5032715 | ACS Appl. Mater. Interfaces 2014, 6, 15132−15139

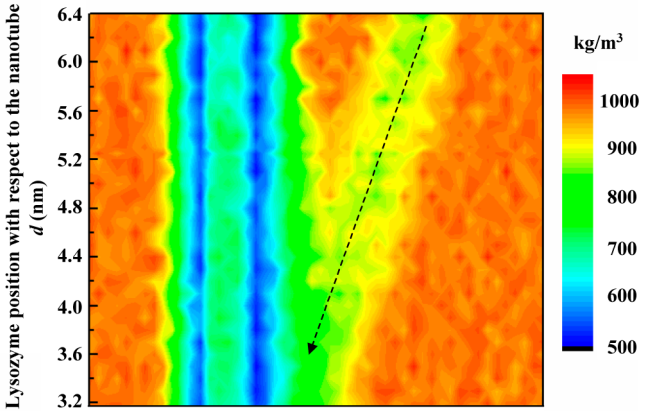

Figure 4. Distribution of water molecules with respective to lysozyme position. Scale bar is for water density: red meaning more water, green representing less water, blue representing the wall of carbon nanotube. For clarity, SHS molecules and lyozyme are not present. As SHS molecules were adsorbed onto the nanotubes as illustrated in Figure 1, the outside region close to the nanotube wall is shown in green. The arrow indicates the regions where the lysozyme remained. The color change along the right side of CNT indicates that, as the lysozyme approaches the CNT, the water molecules are expelled out of the interval region.

adsorption of lysozyme is a spontaneous process, i.e., ΔG is negative, while the values of $-T\Delta S$ of the system is positive, as shown in Figure 3. It can be reasoned that the lysozyme adsorption is dominated by enthalpy.

The attractive interaction between the lysozyme and the SHS molecules $E_{SHS\text{-}Lys}$ is consistently increased (Figure 5).

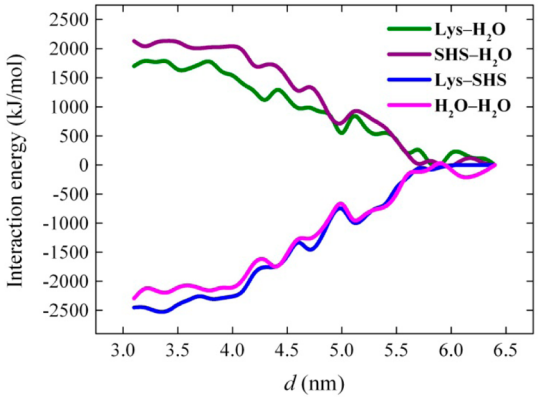

Figure 5. Interaction energy versus distance d.

Meanwhile, the interaction energy between the lysozyme and water $E_{Lys\text{-}H_2O}$ and that between SHS and water $E_{SHS\text{-}H_2O}$ each decrease as the distance d decreases. Note that the most important characteristic in $E_{Lys\text{-}H_2O}$, $E_{SHS\text{-}Lys}$, and $E_{SHS\text{-}H_2O}$ variation curves is that these interactions favor the adsorption of lysozyme on the SHS-CNT. The interaction energy between the lysozyme and SHS $E_{SHS\text{-}Lys}$ is decomposed into electrostatic and van der Waals contributions, denoted by E_{coul}(SHS-Lys) and E_{vdw}(SHS-Lys), respectively. It can be seen clearly in Figure S8b in the Supporting Information that both electrostatic and van der Waals interactions between the lysozyme and SHS are attractive. However, the electrostatic interaction energy between the lysozyme and SHS is larger, in comparison to the van der Waals interaction energy.

Essential Dynamics Analysis. Essential dynamics (ED) analysis[51] was used to further investigate the conformational change of the lysozyme. ED analysis can identify the displacements of groups of residues that are functionally relevant and describe the overall motion of the protein. A subset of the principal eigenvalues and eigenvectors of the residue pair covariance matrix were calculated from MD simulations.[52] The trajectories of the lysozyme were projected onto the first eigenvector.[51,53] In Figure 6, the essential motions

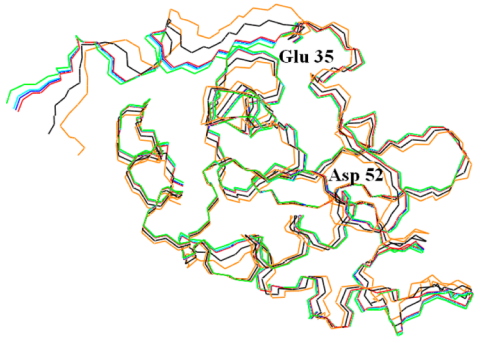

Figure 6. Superposition of six configurations obtained by projecting the motion of the atom Cα onto the first eigenvector. [Colored lines: red = 0 ns, orange = 10 ns, black = 20 ns, green = 30 ns, cyan = 40 ns, and blue = 50 ns.]

of the region are presented, and the superposition of six configurations was obtained by projecting the motion of the atom Cα onto the first eigenvector. The structure displacement with respect to the initial structure is shown in Figure 6. For the active site regions around Glu 35 and Asp 52, the displacement was not significant. The distance between Glu 35 and Asp 52 for measuring the size of the pocket of active site has little change, as illustrated in Figure S11 in the Supporting Information. The results (see Figure 6 and Figure S11 in the Supporting Information) indicate that the conformation around active sites has been well-preserved after lysozyme adsorption onto the SHS−CNT. Other regions with α-helix and β-sheet structures also exhibit little change, indicating that the secondary structure of the lysozyme has been preserved well. This is consistent with the experimental result of CD spectra, as shown in Figure S6 in the Supporting Information, which shows that the red line is close to the black line. The ED analysis is in accordance with the values of radius of gyration of lysozyme, which does not change too much (see Figure S12 in the Supporting Information), indicating that the conformation of the protein has been preserved well during the adsorption process.

Structure of SHS after the Adsorption of Lysozyme. When the lysozyme interacted with SHS, the RMSD values of SHS molecules varied significantly until 40 ns (see Figure S13 in the Supporting Information). By comparing Figures 1 and 7, it was found that the packing of the SHS tails close to the surface of CNT after the lysozyme adsorption is not as dense as that observed before the lysozyme adsorption. Figures 1 and 7, as well as Figure S13 in the Supporting Information, indicate that that the assembled SHS molecules have been reorganizing themselves during the lysozyme adsorption. The reorganized SHS molecules formed a saddle-like structure, which fits the shape of the lysozyme well. In the left and right parts of the saddle-like structure, the SHS molecules aggregated with a larger packing density, in comparison to the density of the SHS

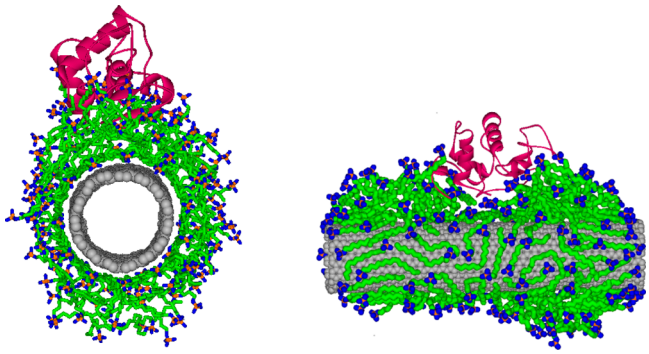

Figure 7. Representative simulation snapshots of equilibrated lysozyme−SHS−CNT; the left panel shows the side view, while the right panel shows the front view.

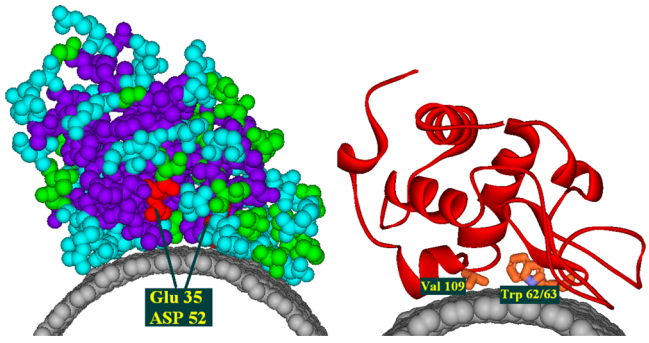

Figure 8. Representative simulation snapshots of equilibrated lysozyme-CNT. Indicated residues are some of the residues that comprise the active-site cleft.

molecules close to the CNT surface. This larger packing density means that more head groups of SHS molecules contact with the lysozyme, interacting with the positively charged residues through Coulombic interactions. The head groups of SHS are located away from the CNT surface in a relative wide range of 8−16 Å, and they display less probability to be perpendicular to the surface (see Figure S14 in the Supporting Information). It can be concluded that the SHS reorganization to form the saddle-like structure is induced mainly by the Coulomb interactions between lysozyme and SHS, as the electrostatic interaction energy is larger than the van der Waals interaction energy (see Figure S8b in the Supporting Information). Because of the well-fitting structure formed and the interactions occurred, the lysozyme is finally positioned with the active-site cleft toward the water phase (Figure 7), facilitating the interaction of substrates with the active site.

To have a comparison, we have performed the MD simulations for the system consisting of lysozyme, CNT, and water. Calvaresi et al. performed MD simulations for lysozyme adsorption on CNTs.[24] Two initial preferential CNT positions were provided through docking procedure. The CNT 1 position is localized in the α-domain of lysozyme, the CNT 2 position is wedged between the α and β domains, in proximity of the catalytic site. In present work, by considering the distributions of hydrophobic residues on the surface of lysozyne and steric hindrance, six initial positions of lysozyme, with respect to the CNT, were selected as indicated in Figure S15 in the Supporting Information. The secondary structure of the lysozyme adsorbed on CNTs has been preserved well, as indicated in the articles.[17,22] However, the lysozyme has some changes according to the simulations in this work. The major changes are that the residues in contact with the CNT surface tend to spread on the surface, as illustrated in Figure S15 in the Supporting Information. Position 4 with the lowest interaction energy (Figure S16 in the Supporting Information) was finally selected for the MD analysis. The hydrophobic interactions between lysozyme and CNT are responsible for the lysozyme adsorption. In the active-site region, most residues are hydrophobic in nature, possibly this is the reason that the lysozyme tend to be adsorbed with the active-site cleft toward the wall of CNT (Figure 8). This final position of the lysozyme is not favorable for the substrate entering into the active site. The MD simulations can explain the experimental results that the conjugate of lysozyme−SHS−CNT retained 83% ± 3% of the free lysozyme. This activity is much higher than that of the lysozyme−CNT, which retained 55% ± 4% of the free lysozyme. Our results are consistent with the experimental results reported by Calvaresi et al.[54] They showed that the C_{60} recognition is highly specific and localized in a well-defined pocket of lysozyme, and enzyme activity assays show that the conjugate of C_{60}−lysozyme retains 53% of activity of the free enzyme.

4. CONCLUSIONS

Carbon nanotubes (CNTs) functionalized with sodium hexadecyl sulfate (SHS) have good dispersibility in water, facilitating the adsorption of proteins, such as lysozyme. The circular dichroism (CD) spectra indicated that the secondary structure of lysozyme has been preserved well upon adsorption. The conjugate of lysozyme−SHS−CNTs retained a higher activity of the free lysozyme than the lysozyme−CNTs conjugate. Molecular dynamics simulations provided the insight into the lysozyme adsorption mechanism. The lysozyme adsorption induces the rearrangement of the assembled SHS forming a saddle-like structure on CNTs, which fits the shape of the lysozyme. Thus, more head groups of SHS interact with the positively charged residues of lysozyme, as indicated by the interaction energy that the electrostatistic interaction is larger than the van der Waals interaction. Because of the combined effect of the formation of saddle-like structure and the interactions between SHS and lysozyme, the lysozyme is finally positioned with the active-site cleft toward the water phase, facilitating the interaction of substrates with the active site. While for the adsorption of lysozyme on nonfunctionalized CNTs, the hydrophobic interactions are responsible for the lysozyme adsorption. In the active-site region, most residues are hydrophobic in nature; this is the main reason that the lysozyme tend to be adsorbed with the active-site cleft toward the wall of CNT, not favorable for the substrate interacting with the active site. The results of this work demonstrate that the SHS molecules as an interfacial substance have a function of adjusting the lysozyme with an appropriate orientation, which is favorable for lysozyme having a higher activity. In addition, compared to the commonly simulated surfactant sodium dodecyl sulfate (SDS),[11] SHS with a C16 tail is longer than SDS. When the head groups of SHS interact with the lysozyme, and the tails remain in contact with the CNT surface, or interact with each other through chain−chain interaction. From this point of view, SHS is preferred.

Two aspects contribute to the fact that the single-walled CNTs can be used to represent the multiwalled CNTs for the MD simulations. When performing the molecular dynamics (MD) simulations for SHS adsorption, we used a packing

density of 2.90 SHS molecules/nm^2 CNT, corresponding to experimental conditions. The packing density is not directly related to the diameter of CNTs. On the other hand, for the adsorption of lysozyme, the simulations started with seven initial orientations (see Figure S7 in the Supporting Information). The equilibrated states of the seven cases show that SHS molecules formed saddle-like structures, induced by the Coulomb interactions between the positively charged residues of the lysozyme and the negatively charged heads of SHS. Visual analysis suggests that the saddle-like structure is parallel to the CNT axis, and the saddle-like structure fits the shape of lysozyme. Thus, the effect of curvature of CNTs on the adsorption of lysozyme is reduced.

■ ASSOCIATED CONTENT

Supporting Information

FTIR, UV-vis and CD spectra, TEM images, additional figures for MD simulations. This material is available free of charge via the Internet at http://pubs.acs.org.

■ AUTHOR INFORMATION

Corresponding Authors

*Tel.: +86-10-64446249. E-mail: fengwei@mail.buct.edu.cn (W. Feng).

*Tel.: +86-10-64423254. E-mail: jipj@mail.buct.edu.cn (P. Ji).

Author Contributions

§These authors contributed equally to this work.

Notes

The authors declare no competing financial interest.

■ ACKNOWLEDGMENTS

This work was supported by the National Science Foundation of China (Nos. 21376021, 21176025), National Hi-tech R&D Program (No. 2014AA022003), and the National Basic Research Program of China (No. 2011CB200905).

■ REFERENCES

(1) Wang, Y. D.; Joshi, P. P.; Hobbs, K. L.; Johnson, M. B.; Schmidtke, D. W. Nanostructured Biosensors Built by Layer-by-Layer Electrostatic Assembly of Enzyme-Coated Single-Walled Carbon Nanotubes and Redox Polymers. *Langmuir* **2006**, *22*, 9776−9783.

(2) Wang, L.; Wei, L.; Chen, Y.; Jiang, R. Specific and Reversible Immobilization of NADH Oxidase on Functionalized Carbon Nanotubes. *J. Biotechnol.* **2010**, *150*, 57−63.

(3) Zhang, B.; Xing, Y.; Li, Z.; Zhou, H.; Mu, Q.; Yan, B. Functionalized Carbon Nanotubes Specifically Bind to α-Chymotrypsin's Catalytic Site and Regulate its Enzymatic Function. *Nano Lett.* **2009**, *9*, 2280−2284.

(4) Gao, Y.; Kyratzis, I. Covalent Immobilization of Proteins on Carbon Nanotubes Using the Cross-linker 1-Ethyl-3-(3-Dimethylaminopropyl) Carbodiimide—A Critical Assessment. *Bioconjugate Chem.* **2008**, *19*, 1945−1950.

(5) Hansen, B. J.; Liu, Y.; Yang, R.; Wang, Z. Hybrid Nanogenerator for Concurrently Harvesting Biomechanical and Biochemical Energy. *ACS Nano* **2010**, *4*, 3647−3652.

(6) Feng, W.; Ji, P. J. Enzymes Immobilized on Carbon Nanotubes. *Biotechnol. Adv.* **2011**, *29*, 889−895.

(7) Tasis, D.; Tagmatarchis, N. Chemistry of Carbon Nanotubes. *Chem. Rev.* **2006**, *106*, 1105−1136.

(8) Coleman, J. N. Liquid-Phase Exfoliation of Nanotubes and Graphene. *Adv. Funct. Mater.* **2009**, *19*, 3680−3695.

(9) Wenseleers, W.; Vlasov, I.; Goovaerts, E.; Obraztsova, E.; Lobach, A.; Bouwen, A. Efficient Isolation and Solubilization of Pristine Single-Walled Nanotubes in Bile Salt Micelles. *Adv. Funct. Mater.* **2004**, *14*, 1105−1112.

(10) Sun, Z.; Nicolosi, V.; Rickard, D.; Bergin, S. D.; Aherne, D.; Coleman, J. N. Quantitative Evaluation of Surfactant-Stabilized Single-Walled Carbon Nanotubes: Dispersion Quality and Its Correlation with Zeta Potential. *J. Phys. Chem. C* **2008**, *112*, 10692−10699.

(11) Xu, Z.; Yang, X.; Yang, Z. A Molecular Simulation Probing of Structure and Interaction for Supramolecular Sodium Dodecyl Sulfate/Single-Wall Carbon Nanotube Assemblies. *Nano Lett.* **2010**, *10*, 985−991.

(12) Chen, R. J.; Bangsaruntip, S.; Drouvalakis, K. A.; Kam, N. W. S.; Shim, M.; Li, Y.; Kim, W.; Utz, P.; Dai, H. Noncovalent Functionalization of Carbon Nanotubes for Highly Specific Electronic Biosensors. *Proc. Natl. Acad. Sci. U. S. A.* **2003**, *100*, 4984−4989.

(13) Yan, Y.; Zheng, W.; Zhang, M.; Wang, L.; Su, L.; Mao, L. Bioelectrochemically Functional Nanohybrids Through Co-assembling of Proteins and Surfactants onto Carbon Nanotubes: Facilitated Electron Transfer of Assembled Proteins with Enhanced Faradic Response. *Langmuir* **2005**, *21*, 6560−6566.

(14) Shim, M.; Kam, N. W. S.; Chen, R. J.; Li, Y. M.; Dai, H. J. Functionalization of Carbon Nanotubes for Biocompatibility and Biomolecular Recognition. *Nano Lett.* **2002**, *2*, 285−288.

(15) McDonald, T. J.; Svedruzic, D.; Kim, Y. H.; Blackburn, H. L.; Zhang, S. B.; King, P. W.; Heben, M. J. Wiring-Up Hydrogenase with Single-Walled Carbon Nanotubes. *Nano Lett.* **2007**, *7*, 3528−3534.

(16) Calvaresi, M.; Zerbetto, F. The Devil and Holy Water: Protein and Carbon Nanotube Hybrids. *Acc. Chem. Res.* **2013**, *46*, 2454−2463.

(17) Nepal, D.; Geckeler, K. E. pH-Sensitive Dispersion and Debundling of Single-Walled Carbon Nanotubes: Lysozyme as a Tool. *Small* **2006**, *2*, 406−412.

(18) Nepal, D.; Geckeler, K. E. Proteins and Carbon Nanotubes: Close Encounter in Water. *Small* **2007**, *3*, 1259−1265.

(19) Bomboi, F.; Bonincontro, A.; La Mesa, C.; Tardani, F. Interactions between Single-Walled Carbon Nanotubes and Lysozyme. *J. Colloid Interface Sci.* **2011**, *355*, 342−347.

(20) Horn, D. W.; Tracy, K.; Easley, C. J.; Davis, V. A. Lysozyme Dispersed Single-Walled Carbon Nanotubes: Interaction and Activity. *J. Phys. Chem. C* **2012**, *116*, 10341−10348.

(21) Nie, H.; Wang, H.; Cao, A.; Shi, Z.; Yang, S. T.; Yuan, Y.; Liu, Y. Diameter-Selective Dispersion of Double-Walled Carbon Nanotubes by Lysozyme. *Nanoscale* **2011**, *3*, 970−973.

(22) Matsuura, K.; Saito, T.; Okazaki, T.; Ohshima, S.; Yumura, M.; Iijima, S. Selectivity of Water-Soluble Proteins in Single-Walled Carbon Nanotube Dispersions. *Chem. Phys. Lett.* **2006**, *429*, 497−502.

(23) Horn, D. W.; Ao, G.; Maugey, M.; Zakri, C.; Poulin, P.; Davis, V. A. Dispersion State and Fiber Toughness: Antibacterial Lysozyme-Single Walled Carbon Nanotubes. *Adv. Funct. Mater.* **2013**, *23*, 6082−6090.

(24) Calvaresi, M.; Hoefinger, S.; Zerbetto, F. Probing the Structure of Lysozyme−Carbon-Nanotube Hybrids with Molecular Dynamics. *Chem.—Eur. J.* **2012**, *18*, 4308−4313.

(25) Shen, J. W.; Wu, T.; Wang, Q.; Kang, Y. Induced Stepwise Conformational Change of Human Serum Albumin on Carbon Nanotube Surfaces. *Biomaterials* **2008**, *29*, 3847−3855.

(26) Feng, W.; Sun, X.; Ji, P. Activation mechanism of *Yarrowia lipolytica* lipase immobilized on carbon nanotubes. *Soft Matter* **2012**, *8*, 7143−7150.

(27) Raffaini, G.; Ganazzoli, F. Protein adsorption on a hydrophobic surface: A molecular dynamics study of lysozyme on graphite. *Langmuir* **2010**, *26*, 5679−5689.

(28) Raffaini, G.; Ganazzoli, F. Surface Topography Effects in Protein Adsorption on Nanostructured Carbon Allotropes. *Langmuir* **2013**, *29*, 4883−4893.

(29) Li, L.; Feng, W.; Ji, P. Dispersion of Carbon Nanotubes in Organic Solvents Initiated by Hydrogen Bonding Interactions. *AIChE J.* **2012**, *58*, 2997−3002.

(30) Tan, H.; Feng, W.; Ji, P. Lipase Immobilized on Magnetic Multi-Walled Carbon Nanotubes. *Bioresour. Technol.* **2012**, *115*, 172−176.

(31) Cavalieri, F.; Micheli, L.; Kaliappan, S.; Teo, B. M.; Zhou, M.; Palleschi, G.; Ashokkumar, M. Antimicrobial and Biosensing Ultra-

sound-Responsive Lysozyme-Shelled Microbubbles. *ACS Appl. Mater. Interfaces* **2013**, *5*, 464−471.
(32) Du, K.; Sun, J.; Song, X. Q.; Chen, H. M.; Feng, W.; Ji, P. J. Interaction of an Ionic Liquid [bmin][CF_3SO_3] with Lysozyme Investigated by Two-dimensional Fourier Transform Infrared Spectroscopy. *ACS Sustainable Chem. Eng.* **2014**, *2*, 1420−1428.
(33) Gordon, J.; Myers, J.; Folta, T.; Shoja, V.; Heath, L.; Onufriev, A. H++: A Server for Estimating pK_as and Adding Missing Hydrogens to Macromolecules. *Nucleic Acids Res.* **2005**, *33*, W368−W371.
(34) Schuttelkopf, A. W.; Van Aalten, D. M. F. PRODRG: A Tool for High-throughput Crystallography of Protein−Ligand Complexes. *Acta Crystallogr., Sect. D: Biol. Crystallogr.* **2004**, *60*, 1355−1363.
(35) Schweighofer, K. J.; Essmann, U.; Berkowitz, M. Simulation of Sodium Dodecyl Sulfate at the Water−Vapor and Water−Carbon Tetrachloride Interfaces at Low Surface Coverage. *J. Phys. Chem. B* **1997**, *101*, 3793−3799.
(36) Hess, B.; Kutzner, C.; Van der Spoel, D.; Lindahl, E. GROMACS 4: Algorithms for Highly Efficient, Load-Balanced, and Scalable Molecular Simulation. *J. Chem. Theory Comput.* **2008**, *4*, 435−447.
(37) Oostenbrink, C.; Villa, A.; Mark, A. E.; et al. A Biomolecular Force Field Based on the Free enthalpy of Hydration and Solvation: The GROMOS Force-Field Parameter Sets 53A5 and 53A6. *J. Comput. Chem.* **2004**, *25*, 1656−1676.
(38) Berendsen, H. J. C.; Grigera, J.R.; Straatsma, T. P. The Missing Term in Effective Pair Potentials. *J. Phys. Chem.* **1987**, *91*, 6269−6271.
(39) Berendsen, H.; Postma, J.; DiNola, A.; Haak, J. Molecular Dynamics with Coupling to an External Bath. *J. Chem. Phys.* **1984**, *81*, 3684−3690.
(40) Essmann, U.; Perera, L.; Berkowitz, M.; Darden, T.; Lee, H.; Pedersen, L. A Smooth Particle Mesh Ewald Method. *J. Chem. Phys.* **1995**, *103*, 8577−8592.
(41) Hung, S. W.; Hsiao, P. Y.; Chieng, C. C. Dynamic Information for Cardiotoxin Protein Desorption from a Methyl-Terminated Self-Assembled Monolayer Using Steered Molecular Dynamics Simulation. *J. Chem. Phys.* **2011**, *134*, 194705.
(42) Torrie, G. M.; Valleau, J. P. Nonphysical Sampling Distributions in Monte Carlo Free-Energy Estimation: Umbrella Sampling. *J. Comput. Phys.* **1977**, *23*, 187−199.
(43) Kumar, S.; Rosenberg, J. M.; Bouzida, D.; Swendsen, R. H.; Kollman, P. A. The Weighted Histogram Analysis Method for Free-Energy Calculations on Biomolecules. I. The Method. *J. Comput. Chem.* **1992**, *13*, 1011−1021.
(44) Youn, S. C.; Jung, D.; Ko, Y. K.; Jin, Y. W.; Kim, J. M.; Jung, H. Vertical Alignment of Carbon Nanotubes Using the Magneto-evaporation Method. *J. Am. Chem. Soc.* **2009**, *131* (2), 742−748.
(45) Sun, Z. Y.; Yuan, H. Q.; Liu, Z. M.; Han, B. X.; Zhang, X. R. A Highly Efficient Chemical Sensor Material for H_2S: α-Fe_2O_3 Nanotubes Fabricated Using Carbon Nanotube Templates. *Adv. Mater.* **2005**, *17* (24), 2993−2997.
(46) Feng, W.; Luo, R. M.; Xiao, J.; Ji, P. J.; Zheng, Z. G. Self-assembly of Sugar-based Amphiphile on Carbon Nanotubes for Protein Adsorption. *Chem. Eng. Sci.* **2011**, *66*, 4807−4813.
(47) Chennamsetty, N.; Bock, H.; Scanu, L. F.; Siperstein, F. R.; Gubbins, K. E. Cosurfactant and Cosolvent Effects on Surfactant Self-assembly in Supercritical Carbon Dioxide. *J. Chem. Phys.* **2005**, *122*, 1−11.
(48) Rubio, D. A. R.; Zanette, D.; Nome, F. Effect of 1-Butanol on Micellization of Sodium Dodecyl Sulfate and on Fluorescence Quenching by Bromide Ion. *Langmuir* **1994**, *10*, 1151−1154.
(49) Smith, P. K.; Krohn, R. I.; Hermanson, G. T.; Mallia, A. K.; Gartner, F. H.; Provenzano, M. D.; Fujimoto, E. K.; Goeke, N. M.; Olson, B. J.; Klenk, D. C. Measurement of Protein Using Bicinchoninic Acid. *Anal. Biochem.* **1985**, *150*, 76−85.
(50) Greenfield, N. J. Using Circular Dichroism Spectra to Estimate Protein Secondary Structure. *Nat. Protocols* **2006**, *1*, 2876−2890.
(51) Amadei, A.; Linssen, A. B. M.; Berendsen, H. J. C. Essential Dynamics of Proteins. *Proteins: Struct. Funct. Genet.* **1993**, *17*, 412−425.
(52) Peters, G. H.; Van Aalten, D. M. F.; Edholm, O.; Toxvaerd, S.; Bywater, R. Dynamics of Proteins in Different Solvent Systems: Analysis of Essential Motion in Lipases. *Biophys. J.* **1996**, *71*, 2245−2255.
(53) Van der Spoel, D.; Vogel, H. J.; Berendsen, J. C. Molecular Dynamics Simulations of *n*-Terminal Peptides from a Nucleotide Binding Protein. *Proteins: Struct. Funct. Genet.* **1996**, *24*, 450−466.
(54) Calvaresi, M.; Arnesano, F.; Bonacchi, S.; Bottoni, A.; Calò, V.; Conte, S.; Zerbetto, F. C_{60}@ Lysozyme: Direct Observation by Nuclear Magnetic Resonance of a 1:1 Fullerene Protein Adduct. *ACS Nano* **2014**, *8*, 1871−1877.